OBSERVATION OF COHERENT OPTICAL TRANSITION RADIATION AND EVIDENCE FOR MICROBUNCHING IN MAGNETIC CHICANES

S. Wesch*, C. Behrens, B. Schmidt, DESY, Hamburg, Germany
P. Schmüser, Universität Hamburg, Germany

Abstract

At the free electron laser FLASH in Hamburg, we have observed coherent visible and infrared radiation from bunches having passed the magnetic bunch compressor chicanes. The spectral distribution was measured from 350 to 1600 nm with high resolution for various settings of the magnet currents in the chicanes. Remarkably, the coherent visible radiation was found to be stronger for uncompressed bunches than for the compressed bunches needed for FEL operation. Additionally, images of the bunches using narrow bandpass filters from 980 to 1600 nm have been recorded.

INTRODUCTION

In the last years COTR from compressed electron bunches has been observed at several FEL accelerator facilities, e.g. [1, 2]. Besides its perturbing effect on transition radiation (TR) based beam diagnostics, the Microbunching Instability, abounding in the coherent light emission, may as well interfere with the FEL process in a malfeasant way.

Microbunching Instability effects in the micrometer regime were previously observed at the FLASH accelerator. By measuring the spectral intensity of coherent transition radiation in the mid- and far-infrared [3], it could be shown that for uncompressed electron bunches, coherent transition radiation (CTR) with maximum intensity around 10 μm is produced. At the shortest wavelength of 3 μm accessible during these measurements, the spectral intensity was higher by a factor of few thousand with respect to the incoherent radiation level. The main goal of the investigations presented here was to complement these measurements in the near-infrared (NIR) and visible (VIS) regime and to study the dependence of the CTR spectra on the strength of the magnetic compressor chicanes (R_{56}), a key parameter in common microbunching models [4, 5, 6].

EXPERIMENTAL SETUP

At FLASH the photoinjector produces electron bunches with lengths of $\sim$4 ps (rms), which are accelerated to 130 MeV, 450 MeV and 1000 MeV in six acceleration modules (ACC). In FEL operation mode, off-crest acceleration in ACC1 and ACC2/3 induces a energy chirp along the bunches and ensures a pathlength difference in the magnetic chicanes BC2 and BC3. Due to the sinusoidal RF field, the longitudinally compressed bunches consists of a leading high-current spike as short as 15 fs (rms) [7] and a long tail. The thus conditioned bunches enter the undulators, generating SASE-FEL pulses down to 6 nm in wavelengths.

* stephan.wesch@desy.de

Accelerator Settings

For most of our measurements, the RF phases of all accelerating modules were set to on-crest so that the electron bunches experience almost no energy chirp. In this uncompressed mode, the bunches are several picoseconds long after the magnetic chicanes, no leading spike is produced and coherent radiation from sharp macrostructures is completely avoided. The final energy after ACC6 was 950 MeV. For comparison, measurements under normal FEL operation conditions were done. The different used linac settings are listed in Table 1.

Table 1: FLASH Linac Settings

n	phases	$R_{56,BC2}$	$R_{56,BC3}$	charge
(a)	FEL	-185 mm	-55 mm	1.00 nC
(b)	on-crest	-185 mm	-55 mm	0.65 nC
(c)	on-crest	-131 mm	-55 mm	0.65 nC
(d)	on-crest	-131 mm	-20 mm	0.65 nC

Changing the dipole currents of the magnetic chicanes varies their R_{56} and thus the trajectory inside the compressors. The resulting path length alteration had to be compensated by adjusting the phases of the subsequent RF modules to preserve the on-crest condition. The accessible range of dipole currents and thus R_{56} was determined by the apertures of the magnetic chicanes.

Instrumentation

To extend our previous measurements down to shorter wavelengths, two commercial spectrometers for the NIR and VIS regime were used. Due to the shortage of available space inside the accelerator tunnel, two different TR screens (labeled OTR1 and OTR2) separated by about 2 m were used to record the VIS and NIR spectra. Both, OTR1 and OTR2 are off-axis screens, which are hit by deflecting a single bunch out of the train with a fast kicker magnet located after ACC6, about 15 m upstream the OTR screens. Interfering edge radiation from the kicker magnet can be estimated to be at the 10^{-2} level integrated over the entire TR screen and is further mitigated since it is not properly focussed into the spectrometers.

The radiation at OTR1 is coupled out through a CVD diamond window and guided through an evacuated beamline to outside the accelerator tunnel. The NIR instrument used here is a commercial spectrometer (Princeton Instruments SP2150) with a 300 lines/mm blazed grating covering the wavelength range $\lambda \in [800,1600]$ nm. The spectrometer is equipped with an InGaAs line array camera (Andor iDUS DU490A 1.7) with almost flat response from 900 to 1700 nm. Inside the tunnel at OTR2, the light passed a viewport (DUV-200) and was focused with an achromat doublet (BAF10/SF10 composite) into an identical spectrometer with 1200 lines/mm blazed grating for the regime $\lambda \in [350,700]$ nm. This instrument was equipped with an image intensified CCD camera with S20 photocathode (PCO Dicam-Pro). Due to the limited free spectral range of the gratings it is not possible to cover the entire range simultaneously. Both instruments need four different settings (central wavelengths λ_c) to cover their indicated spectral range. The spectral resolution depends on the central wavelength, the detected wavelength and the width of the entrance slit, it will be discussed together with the data analysis.

In addition to the spectrometers, two camera systems were used to image the transverse distribution of the electron bunch at the screen OTR2. For the VIS regime, a standard CCD camera (Basler A311f) was installed, for the NIR regime we used an InGaAs CCD camera (XEVA-FPA-1.7-320). The resolution of the cameras were 22 resp. 17 μm/pixel. In front of the NIR camera, four narrow bandpass filters of central wavelengths $\lambda_c \in \{980,1200,1400,1600\}$ nm and $\sigma_\lambda = 10$ nm bandwidth were installed on a remotely controlled filter wheel. Switching between the various instruments at OTR2 (VIS spectrometer, NIR and VIS camera) was done by remotely controlled mirrors and lenses.

MEASUREMENTS

Spectral Distributions

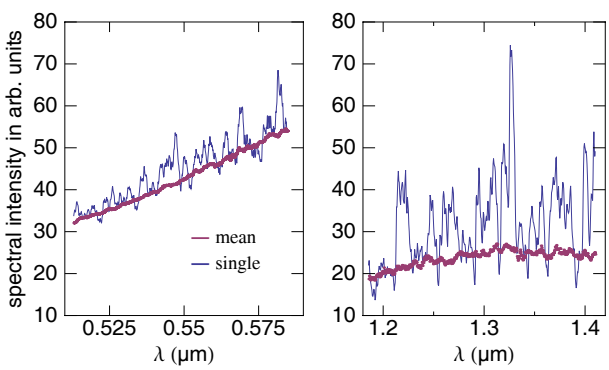

Figure 1: Examples of mean and single-shot TR spectra in on-crest mode. The chicanes were operated at conditions given in Table 1, setting (d).

To determine an unbiased spectrum of the TR source, a variety of wavelength dependent instrumental effects have to be considered. For both spectrometers, quantum efficiencies and the spatial inhomogeneities of the camera systems have been corrected. For the NIR spectrometer, the reflective blazed grating efficiency was calculated with PCGrate-S-6.1 and taken into account. For the VIS spectrometer, no consistent calculation of the grating efficiency could be obtained so far, thus the data are still considered to be preliminary.

As an example, Fig. 1 shows the mean spectral intensity (100 shots) and a single-shot spectrum for the central wavelengths $\lambda_c = 550$ nm and $\lambda_c = 1300$ nm recorded in on-crest mode. In both, the visible and the NIR regime, the single shot spectra exhibit an extremely spiky nature and the intensity in a certain wavelength bin fluctuates considerably from shot to shot. A qualitative analysis of this phenomenon is presented below.

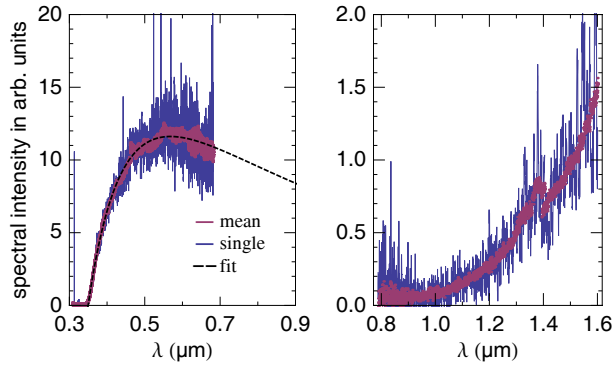

Figure 2: Mean and single-shot TR spectra at FEL operation in the VIS and NIR regime. The dashed line is a fit to the data (see text).

To determine the level of incoherent OTR we used spectra recorded at normal FEL operation. Under these conditions, no indications for coherent radiation in the VIS regime have been reported, neither in the overall intensity nor in the structure of OTR images used for beam diagnostics. This is confirmed by our spectral results presented in Fig. 2. In the VIS regime, the spectrum has a broad maximum around 600 nm, it can be described very well by a shape following λ^{-2} (as expected for completely incoherent emission) and a short wavelength cut-off. The cut-off is expected from the transmission of the optical elements, especially the focussing achromat which basically becomes opaque for $\lambda < 350$ nm. In the NIR regime, the InGaAs detector is not sensitive enough to detect the incoherent radiation level, the rising intensity above 1 μm has to be interpreted as the onset of coherent emission in this operation mode (compressed bunches).

In order to combine the VIS and NIR measurements into a comprehensive spectrum, the unknown ratio of sensitivity of both instruments has to be determined. As shown in Fig. 3, the spectra recorded for all four different machine

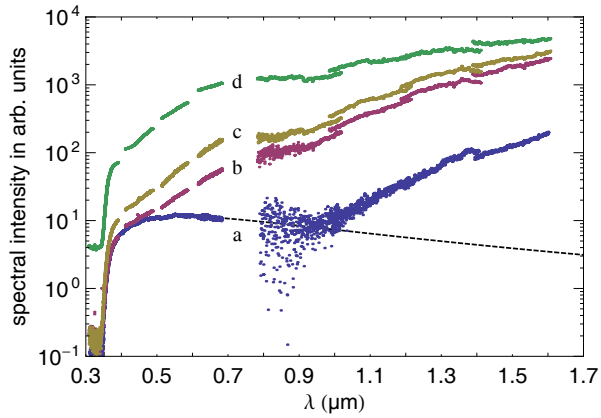

Figure 3: Spectral intensity of different R_{56}'s. The labels (a-d) refer to Table 1. The dashed line represents the incoherent radiation level as determined from the FEL mode data.

settings can be continued smoothly from VIS to NIR by using a single common scale factor. The level of incoherent radiation determined from the FEL mode case is shown as dashed line.

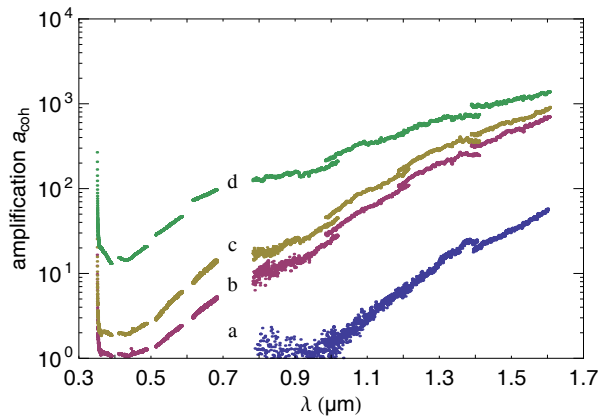

Figure 4: Amplification factors of coherent spectral intensity with respect to the incoherent level. The labels (a-d) refer to Table 1.

If we normalize the spectral intensity to the incoherent level, we get the amplification factor of coherent radiation $a_{\rm coh}$ as shown in Fig. 4. Since this ratio is largely independent of instrumental effects, the data are more reliable than the spectral intensity itself. For normal FEL operation, the onset of coherent radiation is about 1 μm, the intensity then grows exponentially with increasing wavelength (a). Passing the same magnetic chicanes with no energy chirp (on-crest operation), the onset is shifted to about 450 nm with the same exponential slope (b). The coherent intensity in the NIR increases by about a factor 10. Reducing the absolute value of R_{56} in BC2 from 185 mm to 131 mm results in another factor 2 intensity increase with a pronounced "bump" around 700 nm. Reducing additionally $|R_{56}|$ in BC3 from 55 mm to 20 mm increases the coherent radiation in the VIS by another factor 10, the spectrum becomes more flat and exceeds now the incoherent level by a factor 100 in VIS and 1000 in the NIR regime. It should be mentioned that even at 300 nm, where our optics is basically blind, the radiation is clearly measurable.

Fluctuation Analysis

The presence of fluctuations in the radiation produced by short particle bunches is a well known phenomenon and due to the granular structure of the current density. Measuring the fluctuation level has been proposed and used to measure the bunch length [8, 9]. Thus we have to investigate, if the observed fluctuations are in agreement with the expectations from the bunch parameters and how they are influenced in the case of predominant coherent emission.

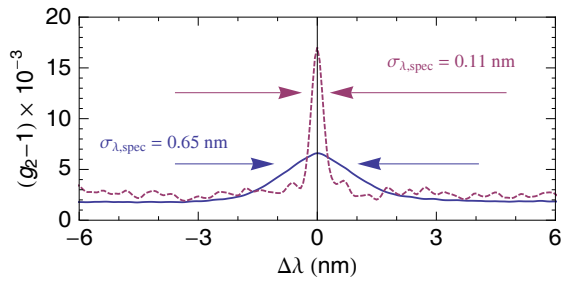

Figure 5: Autocorrelation function for spectrometer slit widths of 730 μm and 145 μm.

To determine the spectral resolution of our measurements, we calculated the intensity autocorrelation function g_2 for single shot spectra measured with two different widths of the spectrometer slit. The result is shown in Fig. 5. Since the width of the autocorrelation function perfectly scales with the slit width, we have to conclude that the width of the observed spectral structures is completely dominated by the instrumental resolution and can not be used for any conclusions about the bunch length (or "correlation length" in the case of coherent emission) directly. Nevertheless, we can use the intensity fluctuations from shot to shot within a certain wavelength band and compare this with model parameters. As an example Fig. 6 shows the distribution of the relative intensity fluctuation (δ in the notation of ref. [10]) at $\lambda_c = 550$ nm for FEL operation (incoherent radiation) and on-crest operation with dominant coherent radiation. For FEL operation, the distribution is almost Gaussian (a Γ-distribution with very high number of modes) with a width of 9% (rms). This is in good agreement with the expected value for incoherent radiation from a Gaussian charge distribution with transverse width $\sigma_\perp = 150\,\mu$m (rms), a resolution of $\sigma_{\lambda,\rm spec} = 0.11$ nm at $\lambda_c = 550$ nm (as measured from the autocorrelation function) and an acceptance angle of γ^{-1} modeling the transition radiation cone. At on-crest configuration with dominant coherent radiation, we observe a Γ-distribution with

much smaller mode number. The black solid line represents the expected distribution for full transverse coherence and the number of longitudinal modes defined by the bunch length (4 ps) and the spectral resolution.

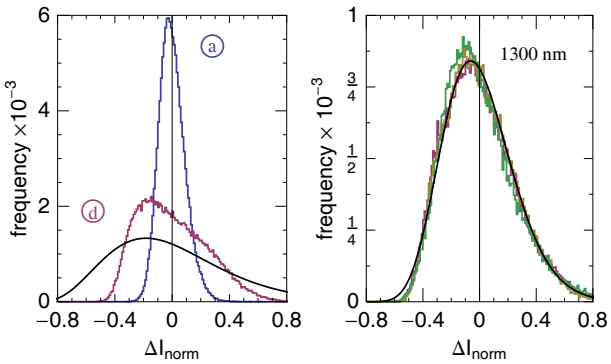

Figure 6: Left: Relative intensity fluctuations for $\lambda_c = 550$ nm for FEL operation (a) and on-crest (d), spectrometer resolution 0.11 nm. Right: Relative intensity fluctuations for $\lambda_c = 1300$ nm for the operation modes (b-c), spectrometer resolution 1.7 nm. The black lines are Γ-distributions as described in the text.

The right plot of Fig. 6 shows the relative intensity fluctuations for the three compressor settings in the NIR regime. The distributions are identical despite the fact that the total intensity varies by more than 2 orders of magnitude. In this case, they follow exactly the expectation for full transverse coherence and a longitudinal mode number of 15 corresponding to 4 ps bunch length.

Transverse Distribution

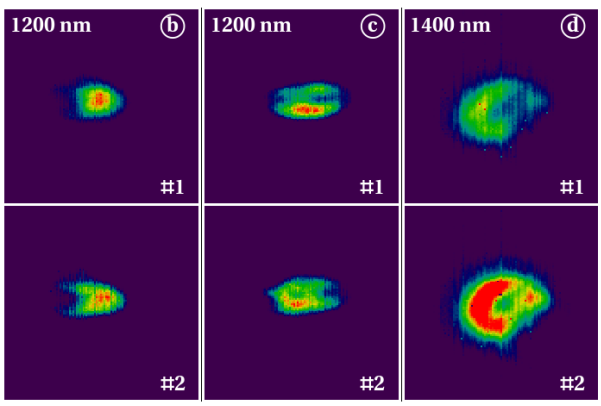

Figure 7: Selection of transverse profiles at different on-crest configurations and various spectral filters. The dimensions of the images are 2×2 mm^2

Complementing the spectral measurements, transverse images of the bunches were taken for various wavelengths in the NIR regime using narrow bandpass filters. The camera for the VIS regime could only be used during normal FEL operation (showing the typical unremarkable transverse beam profile) since it saturated completely for all other machine settings where COTR was present. In Figure 7, a selection of transverse images (2×2 mm^2) for various on-crest settings is shown. The intensity of different configurations are not comparable, since the camera settings had to be individually adjusted to avoid saturation. At standard BC currents (b) and on-crest operation, the beam profile observed at $\lambda_c = 1200$ nm exhibits an almost normal Gaussian shape with minor local fluctuations in intensity and shape despite the fact that the spectral intensity exceeds the incoherent level by already a factor $a_{coh} = 10$. Reducing the R_{56}'s (c,d) and thus increasing the radiation level further, the images disfigure to asymmetric and broader distributions. At long wavelengths, where a_{coh} reaches values of several thousand, almost perfect ring structures are observed as they are expected from homogeneously microstructured bunches. These images look very similar to those observed at SLAC [1] in the visible regime.

CONCLUSION

For the first time we present a comprehensive measurement of the spectral content of coherent radiation produced by micro-structured electron bunches over a large wavelength range from 300 nm - 1600 nm. The intensity of this radiation and thus the level of microbunching strongly depends on the strengths of the magnetic bunch compressors, smaller R_{56} leads to higher intensity and shorter cut-off wavelength. For bunches with correlated energy spread (leading to compression), the coherent emission is strongly suppressed and not measurable below $\lambda = 1000$ nm. The data presented here can be used to benchmark microbunching models and simulations in a stringent way. The spectral measurements are complemented by a large set of transverse beam images for wavelength bands from $\lambda_c = 980$-1600 nm, which should help to get further insight into the microbunching process.

REFERENCES

[1] H. Loos et al., FEL'08, Gyeongju, 2008, THBAU01, p. 488

[2] A.H. Lumpkin, R.J. Dejus, N.S. Sereno, Phys. Rev. ST Accel. Beams **12**, 080702 (2009)

[3] B. Schmidt et al., FEL'08, Gyeongju, 2008, TUPPH068, p. 397

[4] E.L. Saldin, E.A. Schneidmiller, M.V. Yurkov, Nucl. Instrumen. Meth. A **528**, 355 (2004)

[5] D. Ratner, A. Chao, Z. Huang , SLAC-PUB-13392, Sep 24, (2008)

[6] M. Clemens et al., DESY TESLA-FEL-Report 2009-02 (2009)

[7] B. Schmidt et al., EPAC'08, Genoa, 2008, MOPC029, p. 130

[8] M. Zolotorov and G. Stupakov, SLAC-PUB-7132 (1996)

[9] J. Krzywinski et al. , DESY TESLA-FEL-Report 1997-06, 1997, p. 47

[10] F. Sannibale et al., Phys. Rev. ST Accel. Beams **12**, 032801 (2009)